J. Plasma Physics (2005), *vol.* 71, *part* 3, *pp.* 301–313. © 2005 Cambridge University Press
doi:10.1017/S0022377804003095 Printed in the United Kingdom

Ion temperature gradient modes and the fraction of trapped electrons

P. MALINOV† and F. ZONCA

Associazione EURATOM-ENEA sulla Fusione, C. P. 65-00044 Frascati, Rome, Italy
(pm@phys.uni-sofia.bg)

(Received 15 August 2002 and in revised form 3 April 2004)

Abstract. The influence of the trapped electrons fraction on the growth-rate of the ion temperature gradient (ITG) modes is studied numerically for JET relevant conditions. As a possible mechanism for increasing the ITG mode growth rate with an increase in the fraction of trapped electrons, a shift in the real frequency is assumed that leads to less Landau damping. Another possible mechanism is the destabilizing contribution of dissipation effects.

1. Introduction

The ion temperature gradient (ITG) modes are believed to be one of the main reasons for anomalous ion transport in tokamaks. Because of this they have been intensively investigated [1–15].

A useful insight concerning the effect of trapped-electron dynamics on electromagnetic (EM) ITG modes, comes from previous investigations of ideal magnetohydrodynamics (MHDs) and drift type micro-instabilities.

The growth-rate of the high-n ballooning modes decreases when the fraction of the trapped electrons is included in the model [16, 17]. A reduction in the number of the circulating electrons and, consequently, a decrease in the destabilizing parallel-current perturbations provides an explanation for this. Also, for the high-n ballooning modes, the trapped electrons reduce the pressure perturbations. In [17], the growth rate of the interchange-type shear Alfvén mode (called the ITG-driven ballooning mode by the authors) is influenced considerably less than the ordinary MHD ballooning mode. The shear Alfvén mode is connected with the slab-like ITG modes and depends strongly on the ITG.

Recent results by [18] (see also [19–21]), meanwhile, give evidence for the increasing growth rate of the finite-β modified branch of electrostatic (ES) ITG modes when the fraction of the trapped electrons grows.

The explanation for the growth-rate increase of the ITG modes when increasing the fraction of trapped electrons is not fully clarified in the literature, as far as we know. In [16], the author states that the destabilizing mechanism when increasing the trapped-electron fraction is due to non-ideal effects such as magnetic-drift resonances and collisions, and it is quite different from the mechanism responsible for decreasing the ballooning mode growth rate. An intuitive explanation is also given in [21], where it is shown that trapped electrons are destabilizing for the

† Permanent address: Sofia University, Faculty of Physics, BG-1164 Sofia, Bulgaria.

https://doi.org/10.1017/S0022377804003095 Published online by Cambridge University Press

drift mode because they cannot respond adiabatically to local variations of the scalar potential, and, as a consequence, they cannot participate in cancelling charge separations. The eigenfunctions of the ITG modes were studied in [22], when the ITG is changed. It was shown there, that these eigenfunctions spread out somewhat to higher extended angles when the ion temperature gradient is increased, so that the stabilizing effects of the ion transit frequency resonances, or the ion Landau damping, decrease along with the parallel energy convection.

The fluid moment models for Landau damping with application to the ITG mode instability were developed in [23–25]. Extensive investigations of kinetic effects such as Landau damping using the so-called gyro-Landau fluid model were successfully done in [26–28].

Because of the strong influence of the ITG modes on the turbulence drive of anomalous ion transport in toroidal geometry, it is important to further investigate their growth-rate dependence on the fraction of the adiabatically trapped electrons. We have applied known theoretical models – gyro-kinetic and two-fluid models – for investigating the influence of the trapped electrons on the growth-rate of the ITG modes in JET relevant conditions. The main contribution of our work is an applied numerical study of different experimentally relevant dependencies for the ITG mode instability – on the plasma pressure, ITG, finite Larmor radius and the ratio of the characteristic lengths of the pressure and the magnetic field – when the ratio of trapped electrons is varied.

Models of toroidal plasma description

The eigenmode equations used here include final-β (or transverse magnetic perturbation effects) and are obtained as in [29–32]. Furthermore, the trapped electrons are taken into account as in [17, 20]. Thus the quasi-neutrality equation is

$$\delta n_{\mathrm{I}} = (1 - f_{\mathrm{t}})\delta n_{\mathrm{e}} + f_{\mathrm{t}}\delta n_{\mathrm{et}}, \tag{1}$$

where f_{t} is the fraction of trapped electrons and the parallel component of the Ampère's law is

$$\nabla_{\perp}^2 A_{\parallel} = -(4\Pi/c)j_{\mathrm{i}\parallel} - (4\Pi/c)c_{\mathrm{t}}j_{\mathrm{e}\parallel} \tag{2}$$

where c_{t} is the experimentally defined reduction factor of the parallel electron current, which is a factor usually less than $(1 - f_{\mathrm{t}})$, because the parallel velocity is involved in the current moment.

For the fraction of the trapped electrons, we take

$$f_{\mathrm{t}} = [2\varepsilon/(1 + \varepsilon)]^{1/2} \tag{3}$$

as in [33], where ε is the ratio of the minor (cross-sectional) over the big radius of the torus, and for c_{t} we take the approximation $c_{\mathrm{t}} = (1 - f_{\mathrm{t}})$, as in [20]. The expression (3) is yielded when the trapped electrons are assumed to have an approximately Maxwellian velocity distribution [21, 33]. We will drop the contribution of the density response of the trapped electrons in the quasi-neutrality equation in order not to include the trapped electron modes [20]. This is done in order for our investigations to be concentrated on the ITG modes, and not to involve the trapped electron modes, as in [20]. If necessary, the trapped electron modes can straightforwardly be included using the same model for the trapped electrons as that used for the ion response, and adding the term $f_{\mathrm{t}}n_{\mathrm{et}}$ [34]. In the model

https://doi.org/10.1017/S0022377804003095 Published online by Cambridge University Press

used, called the Weiland model in [21], plasma electrons are considered as either deeply trapped or circulating. Circulating electrons are assumed to be fluid-like with adiabatic response to the perturbations in the ES potential [35]. The drift mode perturbation is considered localized on the outboard edge of the flux surface in the midplane [21]. Then only the fraction of the trapped electrons on the outboard edge of the flux surface is important [21]. This provides justification for the ballooning representation and the resultant quasi-local mode analysis on the effect of the trapped electrons that are used.

The perturbed densities and the parallel components of the perturbed current densities are [32]:

$$\delta n_{\rm s} = \int f_{\rm s} d^3v, \quad j_{\rm s\|} = q_{\rm s} \int v_\| f_{\rm s} d^3v \quad (s = i, e)$$

where the distribution function is

$$f_{\rm s} = -q_{\rm s} F_{\rm Ms} \Phi / T_{\rm s} + h_{\rm s} \exp[i(\kappa \times \mathbf{v}) \cdot \mathbf{b}/\Omega_{\rm s}],$$

$\mathbf{b} = \mathbf{B}_0/B_0$, the curvature vector is $\kappa = (\mathbf{b} \cdot \nabla)\mathbf{b}$, and the gyro-frequency of the species s is $\Omega_{\rm s} = q_{\rm i} B_0/(m_{\rm s} c)$, and $q_{\rm i} = e$, $q_{\rm e} = -|e|$.

The gyro-kinetic equation in the ballooning space is used in order to obtain the non-adiabatic response $h_{\rm s}$:

$$(iv_\|/Rq)(\partial/\partial\theta)h_{\rm s} + (\omega - \omega_{\rm Ds})h_{\rm s} = (\omega - \omega_{*\rm sT}) J_0(\delta_{\rm s}) F_{\rm Ms}(q_{\rm s} n_0/T_{\rm s})(\Phi(\theta) - v_\| A_\|(\theta)/c. \tag{4}$$

In the gyro-kinetic equation (4), the diamagnetic frequencies $\omega_{*\rm s}$ are

$$\omega_{*\rm s} = T_{\rm s0}(\nabla n_0 \times \mathbf{B}_0)/\big(q_{\rm s} n_0 B_0^2\big),$$

magnetic drift frequencies $\omega_{\rm Ds}$ are

$$\omega_{\rm Ds} = (T_{\rm s0}/m_{\rm s}\Omega_{\rm s})[\mathbf{B}_0/B_0 \times \nabla B_0)/B_0 + \mathbf{B}_0/B_0 \times \kappa] \cdot \mathbf{k}_\perp (v_\perp^2/2 + v_\|^2)/v_{\rm ts}^2,$$

$$\omega_{*\rm sT} = \omega_{*\rm s}\big[1 + \eta_{\rm s}\big(v^2/v_{\rm ts}^2 - \tfrac{3}{2}\big)\big],$$

$$F_{\rm Ms} = \big(\Pi v_{\rm ts}^2\big)^{-3/2} \exp\big(-v^2/v_{\rm ts}^2\big),$$

$$\delta_{\rm s} = (2b_{\rm s})^{1/2} v_\perp/v_{\rm ts}, \quad 2b_{\rm s} = k_\perp^2 v_{\rm ts}^2/\Omega_{\rm s}^2, \quad \eta_{\rm s} = d\,\ln T_{\rm s0}/d\,\ln n_0,$$

and $v_{\rm ts}$ are the thermal velocities of the species s.

Equation (4) is integrated using the usual conditions $h_{\rm s}(\theta) = 0$ for $\theta \to -{\rm sgn}\,(v_\|)\infty$. Then the perturbed particle and current densities can be obtained [32]. When they are substituted into the quasi-neutrality equation (1) and the parallel component of Ampère's law (2), the following coupled integral eigenmode equations are obtained:

$$\begin{aligned}(1 - f_{\rm t} + \tau)\Phi(k) = \int dk'/(2\Pi)^{1/2}[&(1 - f_{\rm t}) K_{12}^{\rm e}(k,k') A_\|(k') \\ &+ \tau K_{11}^{\rm i}(k,k')\Phi(k') + \tau K_{12}^{\rm i}(k,k') A_\|(k')] \\ k_\perp^2 A_\|(k)/2\tau = \int dk'/(2\Pi)^{1/2}[&-c_{\rm t} K_{21}^{\rm i}(k,k')\Phi(k') - c_{\rm t} K_{22}^{\rm i}(k,k') A_\|(k') \\ &+ K_{21}^{\rm e}(k,k')\Phi(k') + K_{22}^{\rm e}(k,k') A_\|(k')].\end{aligned} \tag{5}$$

https://doi.org/10.1017/S0022377804003095 Published online by Cambridge University Press

In (5) the kernel functions can be obtained as in [32], $\tau = T_e/T_i$, and the other quantities have their usual meaning. The kernel functions for the fluid closure of the model, which are discussed below, are

$$K^i_{11} = -i \int d\xi (2)^{1/2} \omega_{*e} \exp(-i\omega t) \{ \exp[-(k'-k)/4\lambda] / [(1+a)(a\lambda)^{1/2}]$$
$$\times [\omega\tau/\omega_{*e} + 1 - 3\eta_i/2 + 2\eta_i/(1+a)\{1 - (k_\perp^2 + k_\perp'^2)/2\tau(1+a)$$
$$+ k_\perp k'_\perp I_1/(1+a) I_0 \tau_1\} + \eta_i (k'-k)^2/(4a\lambda)] \} \Gamma_0(k_\perp, k'_\perp)$$

$$K^i_{12} = [(k'-k)/2(a\lambda)^{1/2}] K^i_{11}$$

$$K^i_{21} = -[(k'-k)\beta_i/2(a\lambda)^{1/2}]^i_{11}$$

$$K^i_{22} = -[(k'-k)^2 \beta_i/(4a\lambda)]^i_{11}$$

$$K^e_{12} = \{ iq(\Pi\tau)^{1/2} / [S\varepsilon_n (2)^{3/2}] \} (\omega - 1) \operatorname{sgn}(k - k')$$

$$K^e_{21} = -(\beta_i/\tau) K^e_{12}$$

$$K^e_{22} = \beta_i \{ -[(\Pi/32)^{1/2}/(q/S\varepsilon_n)^2] \omega(\omega-1)|k-k'|$$
$$+ (\Pi/8)^{1/2} (q^2 k_\theta / S\varepsilon_n)[\omega - (1+\eta_e)] \operatorname{sgn}(k-k') g(\theta, \theta') \}$$

where

$$g(\theta, \theta') = (S+1)(\sin\theta - \sin\theta') - S(\theta\cos\theta - \theta'\cos\theta')$$
$$+ (\alpha/2)(\theta - \theta' + \sin\theta\cos\theta - \sin\theta'\cos\theta'),$$

$$\lambda = (\xi \omega_{*e} S \varepsilon_n)^2 / (\tau a q^2),$$

$$a = 1 + 2i\xi\omega_{*e}\varepsilon_n g(\theta, \theta')/[(\theta - \theta')\tau],$$

$$k = S k_\theta \theta, \quad k' = S k_\theta \theta',$$

$$k_\perp^2 = k_\theta^2 [1 + (S\theta - \alpha \sin\theta)^2], \quad k_\perp'^2 = k_\theta^2 [1 + (S\theta' - \alpha \sin\theta')^2],$$

$$\Gamma_0 = I_0 [k_\perp k'_\perp / (1+a)\tau] \exp[-(k_\perp^2 + k_\perp'^2)/(1+a)2\tau],$$

$$\alpha = -Rq^2 \, d\beta/dr.$$

The described kinetic model provides the basic equations for the two-fluid approach to the problem that is adopted here. Because of the complexity of the coupled integral eigenmode equations (5), as a step towards understanding the influence of the trapped electron fraction on the ITG modes, a simplification will be used for the numerical calculations as in [21, 34–37]. The same approach and the above-mentioned two-fluid Weiland model were used in [13, 21]. That model has given good results in comparison with the gyro-kinetic model used for drift modes stability analysis. Our model is based on the kinetic approach, discussed above, as in [13, 21]. It uses the two-fluid Braginskii equations [38] and includes particle number conservation and conservation of energy for electrons and ions. That fluid model self-consistently includes different temperatures for electrons and ions, finite

https://doi.org/10.1017/S0022377804003095 Published online by Cambridge University Press

Larmor radii effects, and finite plasma pressure β [21]. Similar fluid models were successfully used elsewhere for investigating Landau damping and other kinetic effects [23–28].

Fluctuating fields and the current density are represented in the stability analysis as $\mathbf{E} = \delta\mathbf{E}$, $\mathbf{B} = \mathbf{B}_0 + \delta\mathbf{B}$, $\mathbf{J} = \mathbf{J}_0 + \delta\mathbf{J}$. Parallel magnetic perturbations, i.e. the compressional Alfvén mode, will be neglected. Then the perturbed fields are

$$\delta\mathbf{E} = -\nabla\delta\varphi - (\partial\delta A_\parallel/\partial t)\mathbf{b}, \quad \delta\mathbf{B} = \nabla \times (\delta A_\parallel \mathbf{b}),$$

where $\delta\varphi$ is the perturbed scalar potential, and $\delta A_\parallel$ is the perturbed parallel vector potential. A perturbed field $\delta\psi$ is introduced, which is related to the parallel vector potential fluctuation $\delta A_\parallel = -i\mathbf{b}\cdot\nabla\delta\psi c/\omega$. As in the covering space the equation $\mathbf{b}\cdot\nabla\delta\psi = -(\partial\delta A_\parallel/\partial t)/c$ is transformed into $(\partial\delta\psi/\partial\chi)/qR = \delta A_\parallel\omega/c$, then $\delta\psi = \int d\chi\delta A_\parallel qR\omega/c$. The parallel electric field perturbation will be $\delta E_\parallel = -i\mathbf{b}\cdot\nabla(\delta\varphi - \delta\psi)$. For our case $|\delta\varphi - \delta\psi|/|\delta\varphi| \approx 1$ so that the coupling with the shear mode will be strong [29].

The electron fluid model that contains EM is obtained as in [39]. The frequency regime

$$v_{\mathrm{ti}} \ll |\omega|/k_\parallel \approx v_{\mathrm{A}} \ll v_{\mathrm{te}}$$

is considered, and it is assumed that the parallel current is carried primarily by the electrons. The electron inertia term is neglected, i.e. using the massless electron response [29]:

$$\delta f_{\mathrm{e}} = F_0 e/T_{\mathrm{e}}\{\delta\varphi - \delta\psi[1 - \omega_{*\mathrm{e}}/\omega(1 + \eta_{\mathrm{e}}(v^2/v_{\mathrm{te}}^2 - \tfrac{3}{2}))]\},$$

where F_0 is taken as Maxwellian:

$$F_0 = (\Pi v_{\mathrm{te}}^2)^{-3/2}\exp(-v^2/v_{\mathrm{te}}^2).$$

From here we can obtain

$$\delta n_{\mathrm{e}}/n_0 = [\delta\varphi - \delta\psi(1 - \omega_{*\mathrm{e}}/\omega)]e/T_{\mathrm{e}0}. \tag{6}$$

Then, from the linearized electron continuity equation,

$$-i\omega\nabla_\parallel\delta n_{\mathrm{e}} = -ien_0(\omega_{*\mathrm{e}} - \omega_{\mathrm{De}})\nabla_\parallel\delta\varphi/T_{\mathrm{e}0} - i\omega_{\mathrm{De}}\nabla_\parallel\delta\mathbf{P}_{\mathrm{e}}/T_{\mathrm{e}0} + (\nabla_\parallel)^2\delta\mathbf{J}_{\mathrm{e}\parallel}/e \tag{7}$$

follows, where $\delta\mathbf{P}_{\mathrm{e}}$ is the electron pressure perturbation and $\delta\mathbf{J}_{\mathrm{e}\parallel}$ is the parallel electron current density perturbation.

Also, using Ampère's law, the following connection between the potentials $\delta\varphi$ and $\delta A_\parallel$ can be obtained:

$$i(\omega - \omega_{*\mathrm{e}})\nabla_\parallel\delta\varphi = [-(\omega - \omega_{*\mathrm{e}})(\omega - \omega_{\mathrm{De}}) - \eta_{\mathrm{e}}\omega_{*\mathrm{e}}\omega_{\mathrm{De}} + v_{\mathrm{A}}^2\rho_{\mathrm{s}}^2\nabla_\parallel(\nabla_\perp^2\nabla_\parallel)]\delta A_\parallel/c, \tag{8}$$

where v_{A} is the Alfvén velocity, v_{s} is the ion-sound velocity, and $\rho_{\mathrm{s}} = v_{\mathrm{s}}/\Omega_{\mathrm{i}}$. It worth mentioning that quite a similar electron response follows from kinetic theory for the electrons of the frequency regime under consideration [17].

The ion fluid model was obtained after [5]. The ion continuity equation is used, including the polarization and stress tensor drifts, and compressibility effects due to the magnetic field curvature. From the ion energy equation, the following density response is obtained:

$$\delta n_{\mathrm{i}}/n_0 = Qe\delta\varphi/T_{\mathrm{i}0}, \tag{9}$$

https://doi.org/10.1017/S0022377804003095 Published online by Cambridge University Press

where $Q = T/N$, and

$$T = \omega(\omega_{\mathrm{Di}} - \omega_{*\mathrm{i}}) + \left(\tfrac{7}{3} - \eta_{\mathrm{i}}\right)\omega_{*i}\omega_{\mathrm{Di}} - 5\omega_{\mathrm{Di}}^2/3 + (\omega - 5\omega_{\mathrm{Di}}/3)[\omega - \omega_{*\mathrm{i}}(1+\eta_{\mathrm{i}})]\rho_{\mathrm{s}}^2\nabla_{\perp}^2/\tau,$$

$$N = \omega^2 - 10\omega_{*\mathrm{i}}\omega_{\mathrm{Di}}/3 + 5\omega_{\mathrm{Di}}^2/3.$$

The ion density response is assumed ES, and does not include EM effects. That ion fluid model has given comparable results to the kinetic theory for high-n ballooning modes [40], and for the ITG modes [41].

The eigenvalue mode equation can be obtained using quasi-neutrality relation (1) and the connection between the potentials (7). Instead of $\delta\varphi$, the more convenient $\Phi = \nabla_{\parallel}\delta\varphi$ will be used. The eigenvalue equation is

$$-v_{\mathrm{A}}^2\rho_{\mathrm{s}}^2\nabla_{\parallel}(\nabla_{\perp}^2\nabla_{\parallel}]\Phi + \{(\omega - \omega_{*\mathrm{e}})(\omega - \omega_{\mathrm{De}}) + \eta_{\mathrm{e}}\omega_{*e}\omega_{\mathrm{De}} - (\omega - \omega_{*\mathrm{e}})^2/[1 - \tau Q/(1 - f_{\mathrm{t}})]\}\Phi = 0, \quad (10)$$

where f_{t} is the ratio of the trapped electrons. The above equation, when transformed into the covering space using the ballooning transformation [42] is a dispersion relation describing the local eigenfrequency on the magnetic field line:

$$(d/d\chi)\left[\left(k_{\perp}^2(\chi)/k_{\theta}^2\right)(d\Phi/d\chi)\right] + \beta[2/(1+1/\tau)](q/\varepsilon_n)^2 V\Phi = 0, \quad (11)$$

where

$$V = (\Omega - 1)[\Omega - \varepsilon_n g(\chi)] + \eta_{\mathrm{e}}\varepsilon_n g(\chi) - (\Omega - 1)^2/[1 - \tau Q/(1 - f_{\mathrm{t}})],$$

q is the safety factor and S is the magnetic shear. The normalization of the frequency is made, as is usual for the ITG modes, with respect to the electron diamagnetic frequency $\Omega = \omega/\omega_{*\mathrm{e}}$. In (11), the parameter

$$\varepsilon_n = \omega_{\mathrm{De}}/\omega_{*\mathrm{e}} = 2L_{\mathrm{n}}/L_{\mathrm{B}}, \quad k_{\perp}^2(\chi) = k_{\theta}^2[1 + (S\chi - \alpha\sin\chi)^2],$$

and $g(\chi)$ represents the poloidal variation of ω_{Ds}:

$$g(\chi) = \cos\chi + (S\chi - \alpha\sin\chi)\sin\chi,$$

where $\alpha = \beta q^2[1 + \eta_{\mathrm{e}} + (1+\eta_{\mathrm{i}})/\tau]/\varepsilon_n$. Equation (11) is the eigenmode equation, which is employed for numerical studies whose results are discussed below. The terms that include kinetic effects are in the factor Q – see (9).

Numerical results

The eigenvalue equation (11) is solved numerically, using a shooting technique based on a fourth-order Runge–Kutta method and Newton method. The usual boundary conditions are used: a trial value of the complex frequency is used for boundary conditions $\Phi(0) = 1$ at extended angle $\chi = 0$, where $\Phi'(0) = 0$. Then the eigenvalue is iterated until the condition $\Phi \to 0$, where $\chi \to \infty$ is fulfilled. In our calculations we have used extended angles up to 25 rad. The eigenfunction $|\Phi|$ as well localized within $\chi < 20$ rad. No significant changes in the eigenfrequency or the field $|\Phi|$ were observed when the range of extended angles was increased up to 50 rad.

For the numerical calculations, parameters of the JET hot-ion discharges #26095 and #26087 are used, as in [20, 43]. An overview for the high-performance JET discharges can be seen in [44].

https://doi.org/10.1017/S0022377804003095 Published online by Cambridge University Press

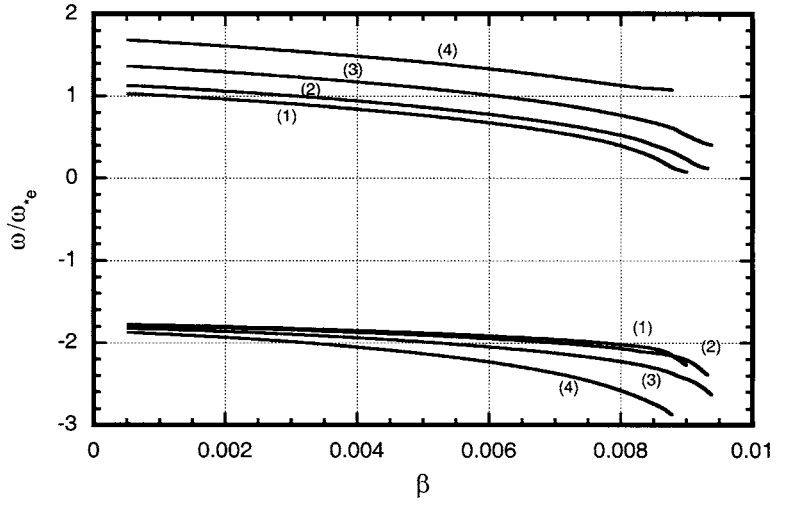


Figure 1. Normalized growth rate γ/ω_{*e} (positive) and real frequency ω/ω_{*e} (negative) as a function of β. $(k_\theta\rho)^2 = 0.1$, $q = 1.5$, $s = 0.5$, $\varepsilon_n = 1$, $\eta_e = \eta_i = 3$, $\tau = 1$. Curves: (1) $f_t = 0$; (2) $f_t = 0.1$; (3) $f_t = 0.3$; (4) $f_t = 0.5$.

The dependence of the growth rate and the real frequency on the plasma pressure β is shown in Fig. 1 for different fractions of trapped electrons. It can be seen that with increasing the fraction of trapped electrons, the real frequency also increases. Here the frequency is negative, as the ITG modes propagate in the ion diamagnetic direction. As shown in [22], the quantities $k_\parallel v_{ti}$ and $k_\parallel v_{te}$ in toroidal geometry are replaced, respectively, by ω_{ti} and ω_{te} – the average transit frequencies of ions and electrons. In realistic tokamak cases, the mode frequency can be such that $|\omega| \leqslant \omega_{ti} \ll \omega_{te}$. Then the ion Landau damping is strong because of the ion transit resonances. In our case, the magnitude of $|\omega/\omega_{ti}|$ can be readily obtained from the adopted frequency normalization, considering that the ratio of the electron diamagnetic frequency over the ion transit frequency is

$$\omega_{*e}/\omega_{ti} = k_\theta \rho q R \tau / L_n = k_\theta \rho q \tau / \varepsilon_n.$$

For the hot-ion JET discharges parameters, we take into consideration that the above frequencies are of the same order, so that the regime described in [29] actually applies. For that regime, the finite core-plasma ion compressibility strongly affects the mode dynamics via resonant interactions with the ion transit motion along the magnetic field lines. The growth-rate of the ITG modes has two main driving parts [45]: a current-driven collisional term γ_c and a collisionless term γ_{cl}, which is connected with the Landau damping. Their ratio is

$$\gamma_{cl}/\gamma_c \approx k_\parallel v_{DE}/\nu_E,$$

where v_{DE} is the plasma electron drift in the presence of density and temperature gradients, and ν_E is the effective electron collision frequency. For typical conditions

https://doi.org/10.1017/S0022377804003095 Published online by Cambridge University Press

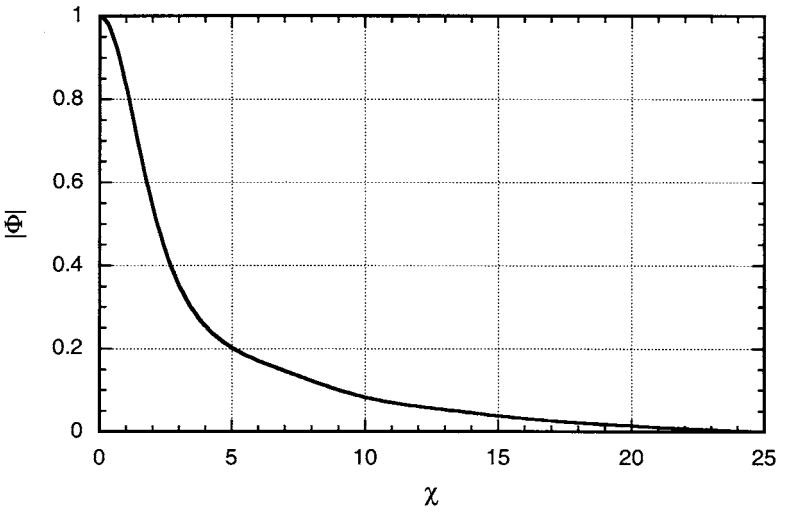


Figure 2. Eigenfunction $|\Phi|$ as a function of the extended angle χ. $(k_\theta \rho)^2 = 0.1$, $q = 1.5$, $s = 0.5$, $\beta = 0.005$, $\varepsilon_n = 1$, $\eta_e = \eta_i = 3$, $\tau = 1$.

of the hot-ion JET discharges, γ_{cl} is an order of magnitude greater than γ_c, so that the Landau damping effects are dominant. When the fraction of trapped electrons is increased, there is a real frequency shift in the direction of higher negative frequencies, as the propagation is in the ion diamagnetic direction. That shift can possibly give less Landau damping, and as a result the growth rate of the ITG modes can be increased. That is the most probable explanation for the increase of the ITG modes growth rate with increasing f_t. Another possible mechanism for that increase is the destabilizing contribution due to trapped-electrons density perturbations through dissipation effects such as collisions or magnetic-drift resonances, discussed in [16]. The modes considered here are the ES branch of the ITG modified by finite β. The finite plasma pressure β makes the real frequency more negative and stabilizes the mode via coupling to the shear Alfvén wave. That stabilization of the ITG modes can be considered as a finite Larmor radius effect that enters through the real mode frequency [20]. It has to be mentioned that the growth-rate curves in Fig. 1 (and some other figures) are not drawn the whole way to zero. This is due to numerical difficulties when the shooting technique is used in a regime close to marginal stability. The numerical results are applicable for hot-ion JET discharges as mentioned above. The tight-aspect spherical tokamaks work at considerably higher β [46–50]. Then the β stabilization would occur via coupling to the shear Alfvén wave. As seen in Fig. 1, the increase of β suppresses the ITG modes more than the increase in the fraction of trapped electrons destabilizes them.

The potential eigenfunction $|\Phi|$ as a function of the extended angle χ is shown in Fig. 2. It can be seen that the mode is well localized within $\chi = 20$ rad. Here, the absolute value of the complex potential is shown as in [20], in contrast to [22] where both the real and imaginary parts of the potential are plotted.

The potential $|\Phi|$ as a function of the extended angle χ for different ratios of trapped electrons f_t is shown in Fig. 3. It was mentioned in [22] that when the ion temperature gradient is increased, the potential eigenfunction is spread out. This effect decreases the stabilization by ion Landau damping (i.e. the ion transit

https://doi.org/10.1017/S0022377804003095 Published online by Cambridge University Press

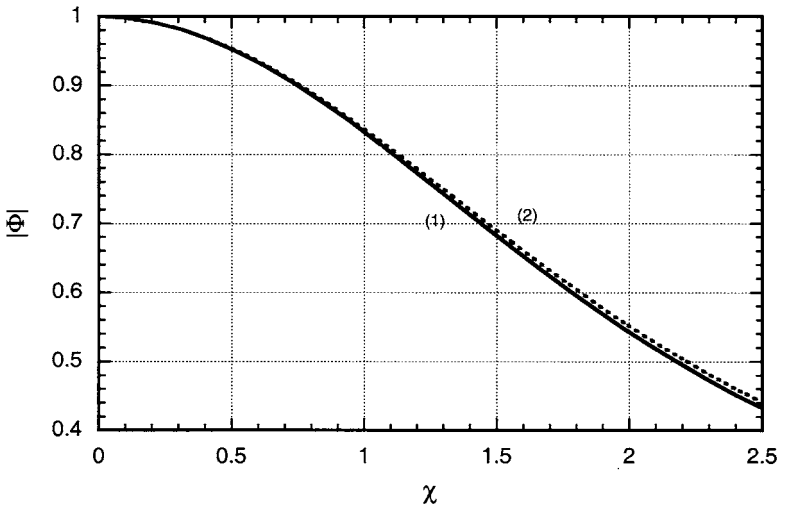


Figure 3. Eigenfunction $|\Phi|$ as a function of the extended angle χ – increased initial part. $(k_\theta \rho)^2 = 0.1$, $q = 1.5$, $s = 0.5$, $\beta = 0.005$, $\varepsilon_n = 1$, $\eta_e = \eta_i = 3$, $\tau = 1$. Curves: (1) $f_t = 0$; (2) $f_t = 0.5$.

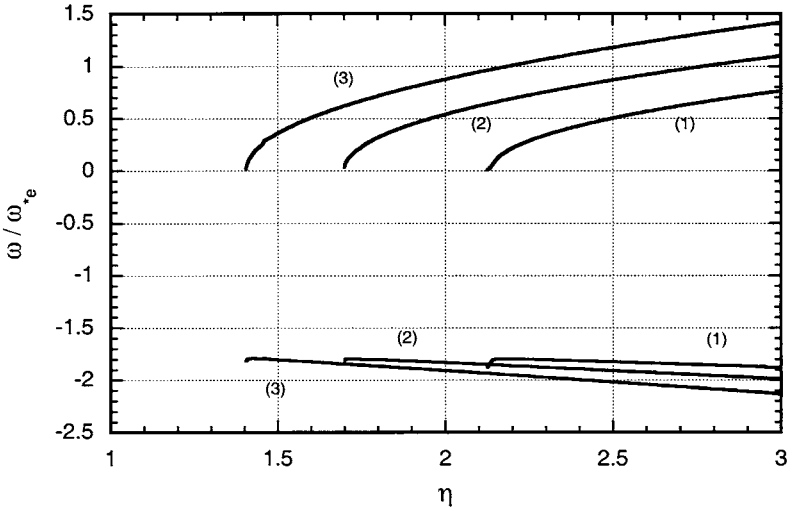


Figure 4. Normalized growth rate γ/ω_{*e} (positive) and real frequency ω/ω_{*e} (negative) as a function of $\eta_e = \eta_i = \eta$. $(k_\theta \rho)^2 = 0.1$, $q = 1.5$, $s = 0.5$, $\beta = 0.005$, $\varepsilon_n = 1$, $\eta_e = \eta_i = \eta$, $\tau = 1$. Curves: (1) $f_t = 0$; (2) $f_t = 0.3$; (3) $f_t = 0.5$.

resonances) and by the parallel energy convection. An increasing ratio of trapped electrons in our case does not give a significant effect for the potential eigenfunction. As can be seen in Fig. 3, the spread of $|\Phi|$ when f_t increases is very small, so that the change of form of the potential eigenfunction is not significant for the investigated phenomenon – increasing the ITG modes growth rate when f_t is increased.

The growth rate and real frequency of the ITG modes are shown in Fig. 4 in dependence on the ion temperature gradient η_i for different trapped electron

https://doi.org/10.1017/S0022377804003095 Published online by Cambridge University Press

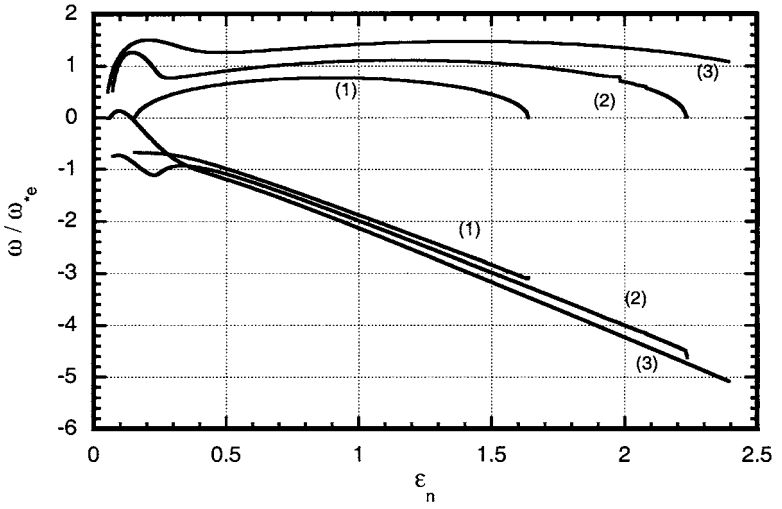


Figure 5. Normalized growth rate $\gamma/\omega_{*\mathrm{e}}$ (positive) and real frequency $\omega/\omega_{*\mathrm{e}}$ (negative) as a function of ε_n. $(k_\theta\rho)^2 = 0.1$, $q = 1.5$, $s = 0.5$, $\beta = 0.005$, $\eta_\mathrm{e} = \eta_\mathrm{i} = 3$, $\tau = 1$. Curves: (1) $f_\mathrm{t} = 0$; (2) $f_\mathrm{t} = 0.3$; (3) $f_\mathrm{t} = 0.5$.

fractions f_t. It can again be seen that increasing f_t results in a shift of the real frequency, which can give a decreased Landau damping and higher growth rate. Also, the lower threshold for the ITG mode is shifted for lower η_i when the fraction of the trapped electrons is increased. That results in an unstable ITG mode with higher growth rate for higher f_t. Here the upper threshold is not shown, because for the usual parameters of the hot-ion discharges of JET, it is well above 15, i.e. it is not interesting from the experimental point of view. However it is also increased when f_t is increased, which gives a higher range in η_i for ITG modes instability.

The dependence of the real frequency and the growth-rate of the ITG modes on the parameter $\varepsilon_n = \omega_{\mathrm{De}}/\omega_{*\mathrm{e}} = 2L_\mathrm{n}/L_\mathrm{B}$ is shown in Fig. 5. Here again the increase in the fraction of trapped electrons gives a shift of the real frequency, which can result in a higher growth rate because of decreased Landau damping. Here it can clearly be seen that the lower threshold of ε_n decreases and the higher threshold increases when f_t is increased, which gives wider range in ε_n of ITG mode instability. The normalization used $\Omega = \omega/\omega_{*\mathrm{e}}$ depends on ε_n, because $\omega_{*\mathrm{e}}$ is proportional to ε_n^{-1}. Therefore, when $\varepsilon_n \to 0$, the normalization factor increases, and in the left part of the figure, the growth rate and real frequency are also visually suppressed because of the normalization used.

The finite Larmor parameter scaling $(k_\theta\rho)$ of the growth-rate and the real frequency is shown in Fig. 6. In particular, for this figure, because the electron diamagnetic frequency also depends on $(k_\theta\rho)$, both the growth rate and the real frequency are multiplied by $(k_\theta\rho)$ in order to cancel out the $(k_\theta\rho)$ dependence via $\omega_{*\mathrm{e}}$. There is a broad maximum for all curves for $(k_\theta\rho)$ between 0.2 and 0.7, and the growth rate at $(k_\theta\rho) = 0.32$ is not very different from the maximum. This justifies the value $(k_\theta\rho)^2 = 0.1$ in our numerical calculations. Again when the fraction of the trapped electrons is increased, there is a shift in the real frequency, which can result in less Landau damping and a higher growth rate. However, with the increase

https://doi.org/10.1017/S0022377804003095 Published online by Cambridge University Press

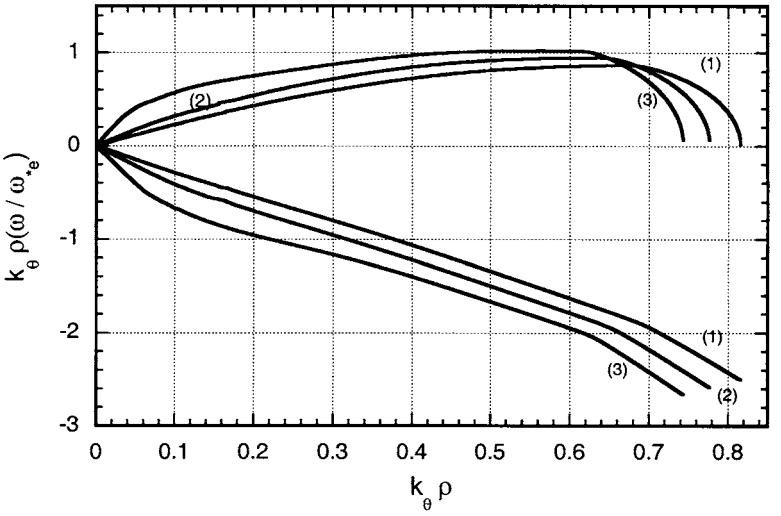


Figure 6. Normalized growth rate γ/ω_{*e} (positive) and real frequency ω/ω_{*e} (negative), both multiplied by $(k_\theta\rho)$ as a function of FLR parameter $(k_\theta\rho)$. $q = 1.5$, $s = 0.5$, $\beta = 0.005$, $\varepsilon_n = 1$, $\eta_e = \eta_i = 9$, $\tau = 1$. Curves: (1) $f_t = 0$; (2) $f_t = 0.3$; (3) $f_t = 0.5$.

of f_t here, the higher threshold on $(k_\theta\rho)$ of the instability is decreased. That gives a reduced number of unstable modes for higher f_t.

Conclusions

In toroidal geometry, the average ion transit frequency in realistic cases can be near to ω_{ti} – the averaged ion transit frequency. That implies that the ion transit resonances, and thus the ion Landau damping will be strong. There is a frequency shift in the direction of higher frequencies in the ion diamagnetic direction (they have a negative sign) for higher ratios of trapped electrons. Because of that shift, the influence of the ion Landau damping can be decreased and, as a result, the growth rate of the ITG modes can be increased. This is the most probable mechanism for the increasing ITG modes growth rate, when f_t increases.

The eigenfunction potential of the ITG modes is well localized up to extended angles of 20 rad. The form of the potential is not significantly spread out for higher extended angles when the fraction of the trapped electrons is increased, so that the phenomenon does not give a considerable effect of increasing growth rate with the increase of f_t.

The ranges of instability both in ITG and the parameter $\varepsilon_n = 2L_n/L_B$ of the ITG modes are enlarged when the fraction of trapped electrons is increased, as the lower threshold is decreased and the upper threshold increased. This gives higher ITG mode instability for higher ratios of trapped electrons f_t.

Increasing f_t gives a lower upper threshold for the finite Larmor radius parameter $(k_\theta\rho)$. This results in less unstable ITG modes for higher f_t.

Acknowledgements

PM gratefully acknowledges the hospitality and encouragement of the staff of ENEA, Frascati, and the financial support from the CNR.

https://doi.org/10.1017/S0022377804003095 Published online by Cambridge University Press

References

[1] Rudakov, L. I. and Sergeev, R. Z. 1961 *Sov. Phys. Dokl.* **6**, 415.

[2] Coppi, B., Rozenbluth, M. N. and Sagdeev, R. Z. 1967 *Phys. Fluids* **10**, 582.

[3] Coppi, B. and Pegoraro, F. 1977 *Nucl. Fusion* **17**, 969.

[4] Guzdar, P. N., Chen, L., Tang, W. M. and Rutherford, P. H. 1983 *Phys. Fluids* **26**, 673.

[5] Jarmén, A., Andersson, P. and Weiland, J. 1987 *Nucl. Fusion* **27**, 941.

[6] Romanelli, F., Chen, L. and Briguglio, S. 1991 *Phys. Fluids* B **3**, 2496.

[7] Kim, J. Y., Horton, W., Choi, D. I., Migliuolo, S. and Coppi, B. 1992 *Phys. Fluids* B **4**, 152.

[8] Horton, W., Lindberg, D., Kim, J. Y., Dong, J. Q., Hammet, G. W., Scott, S. D., Zarnstoff, M. C. and Hamaguchi, S. 1992 *Phys. Fluids* B **4**, 953.

[9] Romanelli, F. and Zonca, F. 1993 *Phys. Fluids* B **5**, 4081.

[10] Kim, C.-B., Horton, W. and Hamaguchi, S. 1993 *Phys. Fluids* B **5**, 1516.

[11] Fröjdh, M., Strand, P., Weiland, J. and Christiansen, J. 1996 *Plasma Phys. Control Fusion* **38**, 325.

[12] Mondt, J. 1996 *Phys. Plasmas* **3**, 939.

[13] Redd, A. J., Kritz, A. H., Bateman, G. and Kinsey, J. E. 1997 *Phys. Plasmas* **4**, 2207.

[14] Bai, L., Fukuyama, A. and Uchida, M. 1998 *Phys. Plasmas* **5**, 989.

[15] Petty, B. C. and Luce T. C. 1999 *Phys. Plasmas* **6**, 909.

[16] Cheng, C. Z. 1982 *Nucl. Fusion* **22**, 773.

[17] Hirose, A., Zhang, L. and Elia, M. 1996 *Phys. Plasmas* **2**, 859.

[18] Falchetto, G. L. and Vaclavik, J. 2002 Global gyrokinetic study of electromagnetic microinstabilities in tokamak plasmas. In: *Proc. IAEA Technical Meeting on Theory of Plasma Instabilities, Kloster Seeon, Germany, 9–11 April 2002*. Kloster Seeon: IAEA.

[19] Brunner, S., Fivas, M., Tran, T. M. and Vaclavic, J. 1998 *Phys. Plasmas* **5**, 3929.

[20] Jarmén, A., Malinov, P. and Nordman, H. 1998 *Plasma Phys. Control. Fusion* **40**, 2941.

[21] Redd, A. J., Kritz, A. H., Bateman, G., Rewoldt, G. and Tang, W. M. 1999 *Phys. Plasmas* **6**, 1162.

[22] Rewoldt, G. and Tang, W. M. 1990 *Phys. Fluids* B **2**, 318.

[23] Hammet, G. W. and Perkins, F. W. 1990 *Phys. Rev. Letters* **64**, 3019.

[24] Hamaguchi, S. and Horton, W. 1990 *Phys. Fluids* B **2**, 1833.

[25] Hamaguchi, S. and Horton, W. 1990 *Phys. Fluids* B **2**, 3040.

[26] Waltz, R. E., Domingues, R. R. and Hammet, G. W. 1992 *Phys. Fluids* B **4**, 3138.

[27] Waltz, R. E., Kerbel, G. D. and Milovich, J. 1994 *Phys. Plasmas* **1**, 2229.

[28] Waltz, R. E., Kerbel, G. D., Milovich, J. and Hammet, G. W. 1995 *Phys. Plasmas* **2**, 2408.

[29] Zonca, F., Chen, L. and Santoro, R. A. 1996 *Plasma Phys. Control. Fusion* **38**, 2011.

[30] Zonca, F., Chen, L., Dong, J. Q. and Santoro, R. A. 1998 *Plasma Phys. Control. Fusion* **40**, 2009.

[31] Zonca, F., Chen, L., Santoro, R. A. and Dong, J. Q. 1999 *Phys. Plasmas* **6**, 1917.

[32] Dong, J., Chen, L. and Zonca, F. 1999 *Nucl. Fusion* **39**, 1041.

[33] Manheimer, W. M. and Lashmore-Davies, C. 1989 *MHD and Microinstabilities in Confined Plasma*. New York: IOP.

[34] Weiland, J., Jarmén, A. and Nordman, H. 1989 *Nucl. Fusion* **29**, 1810.

[35] Bateman, G., Kritz, A. H., Kinsey, J. E., Redd, A. J. and Weiland, J. 1998 *Phys. Plasmas* **5**, 1793.

[36] Nordman, H., Weiland, J. and Jarmén, A. 1990 *Nucl. Fusion* **30**, 983.

[37] Fröjdh, M., Liljestrom, M. and Nordman, H. 1992 *Nucl. Fusion* **32**, 419.

[38] Braginskii, S. I. 1965 *Review of Plasma Physics*, Vol. 1 (ed. M. A. Leontovich). New York: Consultants Bureau, p. 205.

https://doi.org/10.1017/S0022377804003095 Published online by Cambridge University Press

[39] Mondt, J. P. and Weiland, J. 1985 *J. Plasma Phys.* **34**, 143.

[40] Fröjdh, M., Nordman, H. and Jhowry, B. 1995 *Phys. Plasmas* **2**, 4366.

[41] Nilsson, J., Liljestrom, M. and Weiland, J. 1990 *Phys. Fluids* B **2**, 2568.

[42] Connor, J. W., Hastie, R. J. and Taylor, J. B. 1978 *Phys. Rev. Lett.* **40**, 396.

[43] Nordman, H., Strand, P., Weiland, J. and Christiansen, J. P. 1999 *Nucl. Fusion* **39**, 1157.

[44] Jones, T. T. C. and JET Team 1996 In: *Proc. 38th Meeting of the APS Division of Plasma Physics, Denver, CO, 11–15 November 1996*. Denver: APS.

[45] Cap, F. F. 1978 *Handbook of Plasma Instabilities*, Vol. 2. New York: Academic Press, ch. 14, p. 540,

[46] Sykes, A. 2001 *Plasma Phys. Control. Fusion* **43**, A127.

[47] Kaye, S. M., Bush, C. E., Fredrikson, E., LeBlanc, B., Maingi, R. and Sabbagh, S. A. 2003 *Phys. Plasmas* **10**, 3953.

[48] Yavorskij, V. A., Darrow, D., Goloborod'ko, V. Ya., Reznik, S. N., Holzmueller-Steinacker, U., Gorolenkov, N. and Schoepf, K. 2002 *Nucl. Fusion* **42**, 1210.

[49] Voss, G. M., Bond, A., Hicks, J. B. and Wilson, H. R. 2002 *Fusion Eng. Design.* **63–64**, 65.

[50] Connsell, G. F., Ahn, J.-W., Akers, R., Fielding, S. J., Helander, P. Kirk, A., Meyer, H., Tabasco, A., Wilson, H. and Yang, Y. 2003 *J. Nucl. Materials* **313–316**, 804.

https://doi.org/10.1017/S0022377804003095 Published online by Cambridge University Press